Spin conductances and magnetization production in chiral molecular junctions

Richard Korytár,[*,†] Jan M. van Ruitenbeek,[‡] and Ferdinand Evers[¶]

†*Department of Condensed Matter Physics, Faculty of Mathematics and Physics, Charles University, Ke Karlovu 5, 121 16, Praha 2, Czech Republic*

‡*Huygens-Kamerlingh Onnes Laboratory, Leiden University, NL-2333CA Leiden, Netherlands*

¶*Institute of Theoretical Physics, University of Regensburg, D-93050 Regensburg, Germany*

E-mail: richard.korytar@ur.de

Abstract

Motivated by experimental reports on chirality induced spin selectivity, we investigate a minimal model that allows us to calculate the charge and spin conductances through helical molecules analytically. The spin-orbit interaction is assumed to be non-vanishing on the molecule and negligible in the reservoirs (leads). The band-structure of the molecule features four helical modes with spin-momentum locking that are analogous of edge-currents in the quantum spin Hall effect. While charge is conserved and therefore the charge current is independent of where it is measured, - reservoirs or molecule, - our detailed calculations reveal that the spin currents in the left and right lead are equal in magnitudes but with opposite signs (in linear response). We predict that transport currents flowing through helical molecules are accompanied by a spin accumulation in the contact region with the same magnetization direction for source and drain. Further, we predict that the spin-conductance can be extracted directly

from measuring the (quasi-static) spin accumulation - rather than the spin current itself, which is very challenging to obtain experimentally.

Keywords

Chirality-induced spin selectivity, molecular junctions, spintronics

Introduction

Charge currents are routinely measured and analyzed in molecular electronics.[1] The discovery of a family of phenomena that exhibit chirality induced spin selectivity (CISS) has led to a resurge of interest in spin-related phenomena in this field.[2–7] Specifically, experiments report a strong correlation between molecular chirality and a preferred spin direction in systems that exhibit a (nominally) very weak spin-orbit interaction. At present, there is no consensus concerning the explanation of many experimental CISS results.[8]

Motivated by the CISS phenomena, we here address charge and spin currents in chiral molecular junctions within the framework of a minimal model. As a diagnostic tool of the junction's atomic structure, spin currents offer advantages as compared to charge currents: Spin polarized currents can, in principle, be detected in charge-transport measurements within an analyzer-polarizer setup employing, e.g., magnetized leads. However, they are expected to manifest themselves only in the non-linear regime and not in the linear charge conductance $G(\mathbf{M})$.[i] The spin-conductance, on the other hand, is less restricted by Onsager symmetries. It can be inferred, at least in principle, from measuring the pile-up of magnetization, e.g., in source or drain. A brief review of the symmetry properties of transport coefficients is available in the Supporting Information, Sec. S1.

---

[i]As is well known, due to the Onsager relations magnetotransport experiments based on the polarizer-analyzer setup will not detect spin-currents in the linear transport regime: even if a non-vanishing spin-current is flowing, the charge conductance is independent of the magnetization direction $G(\mathbf{M}) = G(-\mathbf{M})$ and therefore insensitive to the flow of spin.

These considerations motivated us and other researchers[9] to investigate a minimal model for a chiral molecule in the presence of spin-orbit interactions. While Ref.[9] has focussed on the effect of contact-enhanced SOI, we adopt the model proposed by Michaeli and Naaman;[10] it exhibits SOI on the entire molecule and has the extra benefit of allowing for an analytical treatment. While Michaeli and Naaman have studied the transmission properties, our focus is on (spin) conductances. As one would have expected, the spin conductance turns out to be non-vanishing due to spin-orbit coupling. As a consequence, the transmitted and reflected currents tend to build up a non-vanishing spin-accumulation near both contacts, source and drain, already in the linear regime.[11] In stationary non-equilibrium the magnitude of induced magnetization is likely controlled by spin-relaxation processes. We predict the orientation of the magnetization in both contacts to be the same, in agreement with requirements of time-reversal invariance (TRI).[9]

Our work is of potential impact for constructing a molecular machine. Since total angular momentum is conserved by the LS-coupling, spin-flip processes exert a mechanical torque that can drive an engine. An analogue driving mechanism based on angular transfer has been investigated in Ref.[12]

Results

Minimal modeling of a helical molecule

Following Michaeli and Naaman[10] we consider electrons bound to a long tube. The left and right side of the tube are of cylindrical shape and represent (semi-infinite) reservoirs; the central region in between takes a helical shape to mimic a chiral molecule, see Fig. 1.

The Schrödinger equation that describes the free motion of a particle inside the helical tube reads

$$\left[-\frac{\hbar^2 \boldsymbol{\nabla}^2}{2m_e} + V_{\mathrm{H}}(\mathbf{r}) + \frac{\mathrm{i}\hbar^2}{4m_e^2 c^2} \boldsymbol{\sigma} \cdot \boldsymbol{\nabla} V_{\mathrm{H}}(\mathbf{r}) \times \boldsymbol{\nabla} \right] \Psi(\mathbf{r}) = E\Psi(\mathbf{r}), \tag{1}$$

where $\mathbf{r}$ is the position vector in three dimensions; $V_H(\mathbf{r})$ denotes an effective single-particle potential that confines the electron to the tube (see Fig. 1) with tube radius d, helical radius R and pitch b. The third term in the square brackets represents the spin-orbit interaction (SOI).

In the limit of small $d/\tilde{R}$ the electronic wavefunction is tightly bound to the helix and the quasi one-dimensional nature of the model becomes manifest; here, $\tilde{R} = \sqrt{(2\pi R)^2 + b^2} > 0$ denotes the distance covered when completing one helical turn. In this limit, the longitudinal and transverse motion approximately decouple and the problem simplifies. Following this idea, a systematic expansion of Eq. (1) in $d/\tilde{R}$ has been performed by Michaeli and Naaman[10] and keeping only leading order terms a minimal model has been derived.

Limit of a narrow tube

Wavefunction factorization

The wavefunction $\Psi(s, \varrho, \theta)$ can be conveniently expressed in a local cylindrical coordinate system: s denotes the longitudinal coordinate (distance along the helix); the motion in the plane normal to the tangential vector $\hat{\mathbf{s}}$ is described by the radial coordinate ϱ, which denotes normal distance from the center line of the tube (Fig. 1), and θ, which denotes the corresponding angular coordinate.

For simplicity, we will assume local rotational invariance in the sense $V_H(\mathbf{r}) = V_H(\varrho)$. In the small $d/\tilde{R}$ limit, the longitudinal and transverse motion nearly decouple,[10] and the wavefunction factorizes,[ii] $\Psi(s, \varrho, \theta) \approx \bar{\Psi}_m(s)\Phi_{N,m}(\varrho)\,e^{im\theta}$. The quantum number $N \in \mathbb{N}_0$ governs the nodal structure of the wavefunction in the radial direction. Due to the stipulated rotational invariance, the $\hat{\mathbf{s}}$-component of the angular momentum, $-i\hbar\partial/\partial\theta$, is a good quantum number; we call it $\hbar m$ and $m \in \mathbb{Z}$. Finally, owing to the presence of SOI, $\bar{\Psi}_m(s)$

[ii]The details of the confinement $V_H(\varrho)$ are not relevant for the main conclusions of our work. Focusing on the lowest-energy eigenstates, we adopt a harmonic approximation $V_H(\varrho) \approx \frac{1}{2}\frac{\hbar^2}{m_e d^4}\varrho^2$: the resulting wavefunctions $\Phi_{N,m}(\theta, \varrho)$ are eigenstates of a 2D harmonic oscillator with m-independent eigen-energies E_N and m restricted to $-N, -N+2, \ldots, N-2, N$.

represents a two-spinor in spin-space.

In leading order, Eq. (1) turns to

$$\hat{H}_{N,m}(s)\bar{\Psi}_m(s) = E\bar{\Psi}_m(s),$$

where

$$\hat{H}_{N,m}(s) = E_N \ - \ \frac{\hbar^2}{2m_{\mathrm{e}}}\left(\frac{\partial^2}{\partial s^2} + \mathrm{i}\frac{2mb}{\tilde{R}^2}\frac{\partial}{\partial s}\right) + \ \hat{H}_{\mathrm{soi}}, \tag{2}$$

with E_N being the energy of the radial and angular motion. The second term on the right is the kinetic energy operator of the longitudinal motion. The third term couples momentum along s with the $\hat{\mathbf{s}}$-component of the orbital angular momentum, $\hbar m$. The origin of this term is geometric, it arises due to a non-zero pitch b of the helix. The last term, $\hat{H}_{\mathrm{soi}}$, is the SOI, which we simplify further in the following.

Spin-orbit coupling term

In the narrow-tube limit an expression for the spin-orbit term was given in the Ref.,[10]

$$\hat{H}_{\mathrm{soi}} = \kappa m\left[\hat{\sigma}_x \sin\left(\frac{2\pi\lambda s}{\tilde{R}}\right) - \hat{\sigma}_y \cos\left(\frac{2\pi\lambda s}{\tilde{R}}\right) - \hat{\sigma}_z\frac{b}{2\pi R}\right] \tag{3}$$

where $\kappa = \lambda(\hbar^4 R)/(4m_e^3 c^2 d^4\tilde{R})$ and $\lambda = +1 \ (-1)$ for a right (left) handed helix.

This expression adopts a transparent form on invoking a Cartesian representation

$$\hat{\mathbf{s}}(s) = -\frac{2\pi R}{\tilde{R}}\sin\left(\frac{\lambda 2\pi s}{\tilde{R}}\right)\hat{\mathbf{x}} + \frac{2\pi R}{\tilde{R}}\cos\left(\frac{\lambda 2\pi s}{\tilde{R}}\right)\hat{\mathbf{y}} + \frac{b}{\tilde{R}}\hat{\mathbf{z}}.$$

With $\mathbf{L} = m\hbar\hat{\mathbf{s}}$ it is easy to see that

$$\hat{H}_{\mathrm{soi}} = \beta\,\mathbf{L}\cdot\boldsymbol{\sigma}, \quad \beta = -\frac{\lambda\hbar^3}{8\pi m_e^3 c^2 d^4}. \tag{4}$$

As s increases along the helix, $\mathbf{L}(s)$ precesses around the z-direction. This spatial depen-

dency of $\mathbf{L}(s)$ is the main entry point of helicity into the quasi-one-dimensional model. The precession of $\mathbf{L}$ invites an analogy with a magnetic moment $\boldsymbol{\mu}$ in a rotating magnetic field with "Zeeman energy" $|\boldsymbol{\mu} \cdot \mathbf{B}| = \hbar\beta m$ and $\mathbf{B} = B[\sin(\Omega s)\hat{\mathbf{x}} - \cos(\Omega s)\hat{\mathbf{y}} + B_z/B\,\hat{\mathbf{z}}]$; s being the effective "time" and oscillation frequency $\Omega = 2\pi/\lambda\tilde{R}$. Motivated by this observation, in the following paragraph we adopt a transformation to the rotating frame.[13]

Non-Abelian gauge transformation

To highlight the conservation of angular momentum in this model, we rewrite (4) introducing ladder operators

$$\hat{H}_{\text{soi}} = \beta \left[\hat{\sigma}_+ \hat{L}_-(s) + \hat{\sigma}_- \hat{L}_+(s) + \hat{\sigma}_z \hat{L}_z \right] \tag{5}$$

$$= \kappa m \left[\hat{\sigma}_+ \, \mathrm{i} e^{-\mathrm{i}\Omega s} - \hat{\sigma}_- \, \mathrm{i} e^{\mathrm{i}\Omega s} - \hat{\sigma}_z \frac{b}{2\pi R} \right] \tag{6}$$

where $\hat{\sigma}_\pm = (\hat{\sigma}_x \pm \mathrm{i}\hat{\sigma}_y)/2$ and $\hat{L}_\pm = \hat{L}_x \pm \mathrm{i}\hat{L}_y$.

In the representation (6), flipping the spin boosts the momentum along the tube axis by a reciprocal lattice vector $2\pi/\tilde{R}$. Alternatively to s, one can label the helical motion with an angle $\delta = \lambda 2\pi s/\tilde{R}$ that takes unique values on the entire real axis; moving up one pitch implies a change of $\delta \mapsto \delta \pm 2\pi$. From this perspective, the phase-factors in (6) boost the angular δ-dependency of the spinor $\Psi(\delta\frac{\lambda\tilde{R}}{2\pi}, \varrho, \theta)$ by an extra factor $e^{\mathrm{i}\delta}$, and in this sense angular momentum is conserved.

While the phase factor in (6) accounts for the conservation of the total angular momentum and therefore is crucial, it also obstructs an easy analytical solution of the model because it is not translationally invariant. The Hamiltonian considerably simplifies after a gauge transformation, $\bar{\Psi}_m(s) \mapsto e^{\mathrm{i}\lambda\hat{\sigma}_z\pi s/\tilde{R}}\bar{\Psi}_m(s)$, and accordingly for operators.[iii]

[iii]All operators transform as

$$\hat{A} \mapsto e^{\mathrm{i}\lambda\hat{\sigma}_z s\pi/\tilde{R}} \hat{A} e^{-\mathrm{i}\lambda\hat{\sigma}_z s\pi/\tilde{R}}.$$

To understand the action of the exponential operator on the spin raising and lowering operators in Eq. (6),

The gauge-transformed Hamiltonian of the spin-orbit interaction follows from (6),

$$\hat{H}_{\text{soi}} \mapsto \hat{H}_{\text{soi}} = -\kappa m \left[\hat{\sigma}_y + \hat{\sigma}_z \frac{\lambda b}{2\pi R} \right]. \tag{7}$$

Whilst the term $\propto \hat{\sigma}_z$ in (6) remains invariant under the transformation, the rotating transverse components of the SOI in (6) collapse onto a single spatial direction, $\hat{\sigma}_y$. The latter direction does not follow from the geometry of the helix, but from our gauge-choice that associates the identity operator with the position $s = 0$.

Minimal model Hamiltonian

The effect of the gauge transformation on the longitudinal momentum operator is given by a spin-dependent "boost" $-\mathrm{i}\partial/\partial s \mapsto -\mathrm{i}\partial/\partial s - \frac{\lambda\pi}{\tilde{R}}\hat{\sigma}_z$. Along with (7) the application of the gauge transformation to the Eq. (2) leads to

$$\hat{H}_{N,m}(s) \mapsto \hat{H}_{N,m}(s) = \frac{\hbar^2}{2m_e}\left(-\mathrm{i}\frac{\partial}{\partial s} - \lambda\frac{\pi}{\tilde{R}}\hat{\sigma}_z + \frac{mb}{\tilde{R}^2} \right)^2 - -\kappa m \left(\hat{\sigma}_y + \hat{\sigma}_z \frac{\lambda b}{2\pi R} \right) \tag{8}$$

where we discarded E_N and a constant $|m|$-dependent energy shift. The analysis simplifies upon introducing dimensionless variables $\hat{H}_{N,m} = \frac{\hbar^2\pi^2}{m_e\tilde{R}^2}\hat{H}'_{N,m}$ and $s = s'\frac{\tilde{R}}{\pi}$, leading to

$$\hat{H}'_{N,m}(s') = \frac{1}{2}\left(-\mathrm{i}\frac{\partial}{\partial s'} - \lambda\hat{\sigma}_z + \tilde{\gamma}m \right)^2 - \tilde{\kappa}m\left(\lambda\hat{\sigma}_y + \hat{\sigma}_z \frac{b}{2\pi R} \right). \tag{9}$$

In the above expression, $\tilde{\kappa} = \frac{\hbar^2 R\tilde{R}}{4\pi^2 m_e^2 d^4 c^2} > 0$ and $\tilde{\gamma} = \frac{b}{\pi\tilde{R}}$.

The $\tilde{\gamma}$-term corresponds to a momentum shift and thus represents a "synthetic" vector potential. It can formally be removed from $\hat{H}'_{N,m}$ by dressing the wavefunctions with a

---

one recalls that $\hat{\sigma}_+$ ($\hat{\sigma}_-$) annihilates spin up (spin down) states. Therefore the transformed operator

$$e^{\mathrm{i}\lambda\hat{\sigma}_z s\pi/\tilde{R}}\hat{\sigma}_+ e^{-\mathrm{i}\lambda\hat{\sigma}_z s\pi/\tilde{R}}$$

annihilates a spin-up state - as it would without being transformed - or equip a spin-down state with two times the same phase factor, i.e. $e^{2\mathrm{i}\lambda s\pi/\tilde{R}}$. As a consequence, the transformation indeed removes the phase factor of $\hat{\sigma}_+$ seen in Eq. (6).

gauge-factor $e^{i\tilde{\gamma}ms'}$,[14] and therefore leaves the spectrum invariant. If $\tilde{\gamma}m$ has a natural interpretation as a vector potential, the term proportional to b/R in the second line of (9) is the corresponding "synthetic Zeeman term". Notice that vector potential, $\tilde{\gamma}m$, and the Zeeman term change sign under $m \mapsto -m$; they do not break TRI because the full Hamiltonian sums over all m.

Dispersion relation

The model Hamiltonian (9) is straightforward to analyze. We focus on the effect of spin flips and therefore discard synthetic fields. Translational invariance of the Hamiltonian (9) suggests a representation in Fourier space

$$\hat{h}_m(k) = \frac{1}{2}\left(k - \lambda\hat{\sigma}_z\right)^2 - \lambda\tilde{\kappa}m\hat{\sigma}_y. \tag{10}$$

The model (10) exhibits a two-band dispersion $E_{m,\alpha}(k)$, where $\alpha = \pm 1$; see Supporting Information, Sec. S2, for explicit expressions.

Fig. 2 shows the dispersion law; the horizontal shift of the two parabolæ, red and blue, reflects the non-Abelian gauge transformation. The spin-orbit term is effective only at the crossing of parabolæ, where it opens a spin-orbit gap, $2|m|\tilde{\kappa}$, as is easily confirmed by degenerate perturbation theory at the crossing point $k = 0$. Chirality-induced spin-selective phenomena are expected to be strong in this region of energies.

In the gap region there remain four ungapped bands, - a factor of two for spin and angular momenta each, - where the spin projection and the sign of the velocity, $\mathrm{d}E_{m,\alpha}(k)/\mathrm{d}k$, are locked. In all four bands, the projection of spin onto the direction of velocity equals $-\lambda$ ("spin-momentum locking"). Such states are termed *helical*, in full analogy to the helicity concept for edge states in the quantum spin Hall effect.[15] The band-structure arising from (10) was also discussed in the context of Rashba quantum wires[16,17] and chiral carbon nanotubes,[18] although the physical origin of the terms of the Hamiltonain was different from our

situation. Specifically, the gap of the minmal model (7) opens due to the SOI term, $-\lambda\tilde{\kappa}m\hat{\sigma}_y$, while in Rashba wires and nanotubes such term originated from a transverse magnetic field.

Spin and charge transport

Molecule bound to straight tubes

To facilitate transport studies, we attach two straight tubes, Fig. 1, which serve as reservoirs. Formally, the reservoirs are included by extending the model (9), so that $\tilde{\gamma}, \tilde{\kappa} = 0$ if $s' < 0$ or $s' > L$. Importantly, the non-Abelian gauge transformation restores translational invariance also after attaching leads provided that it is performed in the reservoirs, too. Similarly, the synthetic vector potential, $\tilde{\gamma}(s')m$, can still be removed by applying a (non-local) gauge factor $e^{im\tilde{\Gamma}(s')}$, with $\tilde{\gamma}(s') = \partial_{s'}\tilde{\Gamma}(s')$.

Basic definitions

A finite bias drop $\mu_{\mathfrak{L}} - \mu_{\mathfrak{R}} = eV$ causes the flow of charge and spin, described by the charge current $I(V)$ and spin currents $I_i^{(\mathfrak{L})}(V)$, $I_i^{(\mathfrak{R})}(V)$ in each lead and each spatial direction $i = x, y, z$. Charge conductance G and spin conductances $G_i^{(\mathfrak{L})}, G_i^{(\mathfrak{R})}$ are defined by the linear response relations

$$I(V) = GV + \mathcal{O}(V^2) \tag{11a}$$

$$I_i^{(\mathfrak{L})}(V) = G_i^{(\mathfrak{L})}V + \mathcal{O}(V^2) \tag{11b}$$

$$I_i^{(\mathfrak{R})}(V) = G_i^{(\mathfrak{R})}V + \mathcal{O}(V^2) \tag{11c}$$

Due to local charge conservation, the charge current is well defined and, in particular, independent of where it is measured along the current flow. In contrast, spin is not locally conserved in the presence of spin-orbit coupling. It is only in the leads of the extended model where (longitudinal) spin-currents are well defined observables. Notice that due to the loss of spin-conservation in the central region, $0 < s < L$, spin-currents in left- and right-

reservoirs, $I_i^{(\mathfrak{L})}$ and $I_i^{(\mathfrak{R})}(V)$, may differ in a quasi-stationary non-equilibrium situation.

We adopt here the following sign convention for the spin currents: The $I_i^{(\mathfrak{L})}$ measures spin entering the junction from the left ($\mathfrak{L}$) contact and $I_i^{(\mathfrak{R})}(V)$ measures spin exiting the junction into the right ($\mathfrak{R}$) contact. This is fully analogous to the definition of the charge current.

Transmissions and Landauer Formulæ

The Landauer formalism relates conductances to the spectral transmission probabilities: for the transmission from $\mathfrak{R}$ to $\mathfrak{L}$, $T_{\sigma\sigma',m}^{(\mathfrak{L}\mathfrak{R})}(E)$, and vice versa, $T_{\sigma\sigma',m}^{(\mathfrak{R}\mathfrak{L})}(E)$, and to the corresponding reflection amplitudes, $R_{\sigma\sigma',m}^{(\mathfrak{L}\mathfrak{L})}(E)$ and $R_{\sigma\sigma',m}^{(\mathfrak{R}\mathfrak{R})}(E)$; see Ref. [19] for an overview. Here, the right (left) subscripts and superscripts of the transmission probability label the quantum numbers of an incoming (outgoing) wave, respectively. For example, $T_{\uparrow\downarrow,m}^{(\mathfrak{R}\mathfrak{L})}$ denotes the probability to transmit an electron with spin down from the left lead to the right one while flipping its spin in eigenchannel m. The charge conductances and the z-components of the spin conductances are given by

$$G = \frac{e^2}{h} \sum_m \sum_{\sigma\sigma'} T_{\sigma\sigma',m}^{(\mathfrak{R}\mathfrak{L})}(E_{\mathrm{F}}), \tag{12a}$$

$$G_z^{(\mathfrak{R})} = \frac{e}{4\pi} \sum_m \sum_{\sigma\sigma'} \sigma T_{\sigma\sigma',m}^{(\mathfrak{R}\mathfrak{L})}(E_{\mathrm{F}}), \tag{12b}$$

$$G_z^{(\mathfrak{L})} = \frac{e}{4\pi} \sum_m \sum_{\sigma\sigma'} (-\sigma) R_{\sigma\sigma',m}^{(\mathfrak{L}\mathfrak{L})}(E_{\mathrm{F}}) \tag{12c}$$

$$= \frac{e}{4\pi} \sum_m \sum_{\sigma\sigma'} \sigma T_{\sigma\sigma',m}^{(\mathfrak{L}\mathfrak{R})}(E_{\mathrm{F}}), \tag{12d}$$

where E_{F} indicates the Fermi energy (the Supporting Information, Sec. S5, offers a standard derivation within the scattering formalism). The expression for G chosen here emphasizes transmission of all spin species from left to right. From that expression the right spin conductance is obtained by multiplication by $\frac{1}{e}\frac{\hbar}{2}\sigma$ in the right lead. The left spin conductance expressed in the Eq. (12c) can then be understood as due to the reflected flux in the $\mathfrak{L}$-lead.

Particle conservation (unitarity, see Supporting Information, Sec. S4), leads to the equivalent form, Eq. (12d).

Transport Results

We address the transport problem by calculating the scattering matrix using conventional wavefunction matching. In this process, angular momentum m matches at the two interfaces: it is conserved in the scattering process; for further details see Supporting Information.

As example we focus on $N = 1$, so that $m = \pm 1$. We further continue to ignore the effect of the synthetic fields. In passing, we briefly mention that their effect is to assign a preferred spin direction, up or down, to a given angular momentum m. Hence, they will result in a circulating (transverse) spin current. In the following our focus is on the longitudinal currents.

The energy dependence of the resulting conductances for charge and spin in this model is displayed in Fig. 3. We offer a few comments:

- With E_{F} well outside the spin-orbit gap, the effect of spin-orbit coupling is small and translational invariance is hardly broken. In this case, back-scattering is weak and the (charge) conductance reaches a maximum of four conductance quanta reflecting two spin and two orbital ($m = \pm 1$) channels.

- In the off-gap regime mesoscopic oscillations are visible. The oscillation frequency (in E_{F}) is seen to decrease with the inverse length, L^{-1} and therefore we assign the oscillations to Fabry-Pérot interference.

- With E_{F} inside the spin-orbit gap, backscattering inside the the wire is suppressed and the Fabry-Pérot oscillations quickly die out.

- In the in-gap regime, electrons can tunnel via two evanescent modes that result from the two 'gapped' bands. Accordingly, the charge conductance in the middle of the gap approaches 2 conductance quanta from above.

- The absolute value of the spin conductances in either one of the leads approaches $2\frac{e}{4\pi}$. This can be understood from Fig. 2: in the spin-orbit gap the right (or left) moving modes have identical spin regardless of m, *i.e.* there are two channels distinguished only by the orbital angular momentum.

- Importantly, the spin conductances are non-zero for energies even far from the spin-orbit gap, where the oscillations peak at $\approx 0.2\frac{e}{4\pi}$. It can be shown that that $G_x^{(\mathfrak{L},\mathfrak{R})}(E_{\mathrm{F}}) = 0$ for any E_{F} since the Bloch functions have zero average $\hat{\sigma}_x$. Moreover, $G_y^{(\mathfrak{L},\mathfrak{R})} = 0$ because the expectation values of $\hat{\sigma}_y$ change sign along with the sign change of m (see Fig. 2), while the lead Hamiltonian is m-independent. In other words, the y components of outgoing waves exactly cancel upon the summation over m.

- Remarkably, the $\mathfrak{L}$ and $\mathfrak{R}$ spin conductances differ only up to a sign. By combining TRI and left-right reflection it is possible to derive relations between scattering matrix elements that lead to the exact identity $G_z^{(\mathfrak{R})} = -G_z^{(\mathfrak{L})}$ at any energy. (See Supporting Information, Sec. S4,S5 for the details of this symmetry analysis.) In realistic molecular junctions a symmetry of couplings to the left and right leads can not be expected. We show in the next section that in this more general situation, the magnitude of $G_z^{(\mathfrak{R})}$ and $G_z^{(\mathfrak{L})}$ no longer is the same, while the sign is still opposite due to TRI.

Qualitative understanding of spin transport

A frequent misconception

We begin the discussion by addressing a common misconception of the minimal model: Fig. 2 is frequently interpreted as predicting a nonzero spin current even in equilibrium. Indeed, Fig. 2 seems to suggest that for a Fermi level situated in the spin-orbit gap there is an excess of spin-up right movers (velocity $\mathrm{d}E_{m,\alpha}(k)/\mathrm{d}k > 0$) over spin-down right movers. Taken at face value this observation would imply that due to the wire connecting $\mathfrak{L}$ and $\mathfrak{R}$ reservoirs, both reservoirs would become magnetized at equilibrium. Clearly, such a

transport of magnetization is violating the second law of thermodynamics. The vanishing of equilibrium spin currents is a rigorous consequence of unitarity, see Supporting Information, Sec. S5. The fact that spin transport can not be derived from the band-structure alone is known in the field of two-dimensional materials, see Sec. 4.1 of Ref.[21] for a review. The paradox will be resolved on a more intuitive level in the subsequent discussion.

Long helix limit

We consider $\lambda = -1$ and the limit $L \gg d, R$ and Fermi energy, E_{F}, inside the spin-orbit gap. In this limit, at observation points deep inside the one-dimensional wire all up-spin fermions flow one direction, while all down-spin fermions flow into the other direction, see Fig. 2. We infer that $T_{\downarrow\downarrow,m}^{(\mathcal{L}\mathcal{R})}, T_{\uparrow\uparrow,m}^{(\mathcal{R}\mathcal{L})} \simeq 1$; there is no spin-flip inside the wire. On the other hand, deep inside either reservoir the spin-orbit gap vanishes. Therefore, spin-up and spin-down currents flow alike in either direction. It is easy to see that both limits match if $R_{\uparrow\downarrow,m}^{(\mathcal{L}\mathcal{L})}, R_{\downarrow\uparrow,m}^{(\mathcal{R}\mathcal{R})} \simeq 1$.

The situation is illustrated in Fig. 4(a). The central region of the junction shows counter-propagating electrons with opposite spin, as suggested by Fig. 2. These modes are properly interpreted as carrying a conductance quantum for charge, because charge is conserved inside the wire; hence, in Fig. 3 the conductance is seen to be $G \approx e^2/h$ per angular-momentum channel inside the gap. These same modes are not properly interpreted in terms of spin-conductances, however, because spin is not conserved inside the wire.

The propagation pattern of current channels in the leads is also displayed in Fig. 4(a); the matching condition at the interface shown there follows from bulk limits. Since spin is conserved inside the reservoirs, the channel pattern may be interpreted in terms of spin currents. As one would expect, there are no net spin currents inside the reservoirs in equilibrium, because the propagating spin-current is exactly compensated by the (reflected) counter-propagating current.

Upon applying a finite bias, states with energy inside the bias window are incoming only from one reservoir. In this case a spin current of one spin-conductance quantum (per angular

momentum channel) survives inside the reservoirs. Also with respect to spin-conductances the Fig. 4(a) and Fig. 3 provide a consistent picture.

The qualitative discussion given here is fully backed up by an explicit calculation of all scattering probabilities; for explicit results, we refer the reader to the Supporting Information, Figure S2.

Reservoirs accumulating spin

An implication of spin-flip scattering is that both reservoirs accumulate spin in the presence of a current flow. To see how this happens we once again consult Fig. 4(a). For a charge current flowing from $\mathfrak{L}$ to $\mathfrak{R}$, the drain acquires a spin up magnetization (red). Simultaneously, the incoming flow of spin down particles (blue) is reflected and spin flipped, so that the $\mathfrak{L}$-lead acquires a spin up magnetization (red), too. The observation represents a one-dimensional analogue of the Rashba-Edelstein effect.[22]

The parallel magnetizing of both leads is formally expressed by the anti-symmetry of spin conductances

$$G_z^{(\mathfrak{R})} = -G_z^{(\mathfrak{L})}. \tag{13}$$

The identity can be proven to hold under general conditions (*e.g.* at arbitrary energy) provided the coupling to both leads is symmetric. We present a formal proof in the Supporting Information, Sec. S5. Importantly, if mirror symmetry is broken, the sign of conductances remains opposite, as we demonstrate in Sec. .

Comparison to a spin filter

For further illustration, we confront the spin-flip scattering in the helical junction with the more familiar case of a magnetized junction that operates as a spin-filter, Fig. Fig. 4(b). Also in this archetypal situation the reservoirs accumulate spin, however they do so in opposite directions (see the schematics of scattering in Fig. 4). The key difference to the previous case is that spin is conserved everywhere, so that the (minority) spins removed from the source

14

accumulate in the drain.

Magnetizing reservoirs with imperfect contacts

Realistic molecular junctions exhibit contact resistances that are not included in the minimal model. To investigate the effect of contact imperfections we add a potential term to the $\mathfrak{L}$ contact,

$$v(s') = c\,\delta(s') \cdot \hat{\sigma}_0. \tag{14}$$

This potential barrier is readily built into the scattering formalism as a modification of the matching conditions between the wire and the leads (Supporting Information, Sec. S3).

Fig. 5 displays the conductances for increasing barrier strength. The charge conductance exhibits a gradual cross-over from the transparent, weak-barrier limit, $c \ll 1$, to the strong-barrier limit, $c \gg 1$, in which the transmission grows linearly with E_{F}. Concomitantly, the spin-conductances evolve in a strikingly asymmetric fashion. For qualitative insight to the strong barrier limit we consult again Fig. 4(a). For a current flowing from $\mathfrak{L}$ to $\mathfrak{R}$ and E_{F} inside the spin-orbit gap, the barrier suppresses the transmitted current and spin-flip processes alike; hence, $G_z^{(\mathfrak{L})}$ is strongly suppressed inside the source. Conversely, the spin-current flowing in the drain equals the transmitted current (in units of the conductance quanta). Our argument implies that the spin conductances continue to exhibit opposite signs in the presence of asymmetries. Therefore, we propose that the property of source and drain to magnetize into the same direction upon a current flowing is a general result robust with respect to generic deformations of the minimal model (14).

Induced spin and charge densities in the contact

We supplement the transport results with expressions for the charge and spin density in the $\mathfrak{L}$-lead ($s < 0$) in linear response. The latter quantities will be given in units of e

and $\hbar/2$, respectively. Our formulæ follow from scattering theory and are thus independent on the microscopic details of the Hamiltonian. The details of the derivation are moved to Supporting Information, Sec. S6, for the sake of brevity.

The charge density evaluates to the expression

$$n(s) = n(s)\Big|_{V=0} + V \varrho_{\mathrm{L}}(E_{\mathrm{F}}) \left[\left(4 - \frac{h}{e^2}G\right) + 2 \sum_m \mathrm{Re}\left\{ e^{-\mathrm{i}2qs} r_{\uparrow\uparrow,m}^{(\mathfrak{L}\mathfrak{L})} \right\} \right]_{E=E_{\mathrm{F}}} + \mathcal{O}\!\left(V^2\right). \quad (15)$$

where $r_{\uparrow\uparrow,m}^{(\mathfrak{L}\mathfrak{L})} = r_{\downarrow\downarrow,-m}^{(\mathfrak{L}\mathfrak{L})}$ has been used reflecing TRI (see also Supporting Information, Sec. S6). The first term is the equilibrium charge density; as shown in Supporting Information, Sec. S6.2, it reveals a familiar contact Friedel oscillation caused by quantum interference with reflected waves in a Fermi ground-state.

In the linear response term in (15) we factored out the expression

$$\varrho_{\mathrm{L}}(E_{\mathrm{F}}) = \frac{1}{2\pi} \sum_{q>0} \delta\!\left(E_{\mathrm{F}} - \frac{q^2}{2} \right) = \frac{1}{4\pi^2 q_{\mathrm{F}}}, \quad (16)$$

being a (homogeneous) local density of states of right movers (per spin) in a single channel homogeneous wire. The square brackets in Eq. (15) contain two terms: a homogeneous (s-independent) term, $\left(4 - \frac{h}{e^2}G\right)$, represents the enhancement of the charge-density that is associated with the reflected particles. The reflection-induced enhancement of the charge density also leaves a trace in the Friedel-oscillations, which is expressed by the second term.

Notice that unlike spin-conserving processes, spin-flip processeses, such as incorporated by $r_{\downarrow\uparrow,m}^{(\mathfrak{L}\mathfrak{L})}$, do not contribute to the oscillating term in (15) because the superposition of two probability currents with opposite spins has no cross (interference) term. Spin-flip terms do enter the conductance, G, of course.

The induced spin density in the left lead reads

$$n_z(s) = -V \varrho_{\mathrm{L}}(E_{\mathrm{F}}) \frac{4\pi}{e} G_z^{(\mathfrak{L})} + \mathcal{O}\!\left(V^2\right); \quad (17)$$

there is no spin density in equilibrium because of TRI. The (linear) spin imbalance represents the the loss of spin-density associated with the transmitted spin-current. For this reason, Eq. (17) implies that a measurement of the linear response of the local spin-density yields (up to trivial factors) the transport coefficient $G_z^{(\mathcal{L})}$. Notice that in striking contrast to the charge density, the spin density does not display Friedel oscillations even in linear response; ultimately, as we show in the Supplementary Information, the reason is TRI.

We further note that the current-induced spin-accumulation, (17), goes hand in hand with a spin-split chemical potential if a self-consistent description of the quasi-static non-equilibrium situation is employed:[23]

$$\mu_\uparrow^{(\mathcal{L})}(V) - \mu_\downarrow^{(\mathcal{L})}(V) = -V\frac{\pi}{2e}G_z^{(\mathcal{L})} + \mathcal{O}(V^2);$$

(18)

the formula follows from (17) and is also derived in the Supplementary Information, Supporting Information, Sec. S6. We offer two comments on this expression: First, the coefficient multiplying V can reach $\frac{1}{4}$ if E_F lies in the SOI gap, *i.e.* the spin accumulation is non-perturbative in the SOI strength. Second, assuming that the reservoirs ultimately relax spin (and charge), but do not introduce backscattering, the spin accumulations can be measured in the vicinity of the contact by a four-terminal setup.

Further remarks

- The (experimental) measurement of spin currents and spin accumulation is a central topic in the field of *Spintronics*.[24,25] In particular, the possibility of spin accumulation near interfaces between materials with and without spin-orbit interaction is well understood;[26] the results we here report on the minimal level confirm the validity of the general picture down to the molecular scale.

  In Sec. 2 we have mentioned that the bands for energies in the spin-orbit gap are analogous to edge states associated with a quantum spin Hall device. As a consequence, the

minimal model exhibits spin-momentum locking with the consequence that backscattering off defects is suppressed. In other words, we expect that our transport results are robust against weak (non-magnetic) disorder.

- Recently, a related work on parallel spin-accumulation and spin transport has been published.[9] The tight-binding chain investigated by these authors is essentially equivalent to our toy model with a distinctive difference: in Ref.[9] the SOI is confined to the contact bond, only, while in our toy model the SOI is a property of the molecule and non-vanishing along the entire helical structure.

  The spin conductances reported in Ref.[9] show the same symmetry, $G_z^{(\mathfrak{L})} = -G_z^{(\mathfrak{R})}$, as in our work. However, the energy dependences of the spin conductances exhibit pronounced differences: $G_z^{(\mathfrak{L}/\mathfrak{R})}(E)$ in Ref.[9] does not exhibit a fixed sign; in our case it does, so that the sign of the spin accumulation is independent of the Fermi energy. This difference can be traced back to the different ways how SOI is implemented; it may, at least in principle, be used to discriminate one situation from the other, experimentaly.

- It is well-known in Spintronics that spin conductances are non-zero in junctions with multiple conduction channels only (see Supporting Information, Sec. S1, Principle 1). In our model, the absence of spin polarization for a single channel is immediately obvious by setting $m = 0$ in Eq. (9). Molecular junctions generically exhibit multiple channels and are thus prepared for hosting spin currents (*e.g.* see Ref.[27] for a channel analysis of helical peptides). Frequently employed molecular linker units (*e.g.* thiol groups linked to Au) effectively suppress all conduction channels but one. Moreover, the generation of significant spin currents benefits from two conduction channels of similar transmission probabilities, which in turn requires quasi-degenerate molecular orbitals. To favor such conditions, linker-free benzene-type structures are natural candidates. They can be functionalized with heavier elements (see *e.g.* Ref.[28]) to boost the spin-orbit coupling and promote chirality.

Summary and conclusions

We have investigated charge and spin transport in a minimal model of a helical molecule with spin-orbit coupling attached to two spin-conserving leads. The minimal model was first devised by Michaeli and Naaman and allows for a full analytic treatment of transport properties. While the earlier authors have focussed on spin polarizations, we calculated the full conductance matrix, including charge and spin conductances.

The band-structure of the minimal model hosts four helical bands that exhibit spin-momentum locking. We first clarify the connection between transport properties and band-structure. In particular, first glances could suggest the existence of an equilibrium spin current, which sometimes is used as an argument against the validity of the model. We explain the origin of the misunderstanding, which results from neglecting the contact scattering that always exists in a transport geometry. In actuality, there is no equilibrium spin transport in this model.

Our explicit calculation of charge and spin conductances in the Landauer formalism show that the spin conductance reaches a maximum $(e/2\pi)$ for energies inside the gap, corresponding to 2 fully polarized conduction channels. Outside the gap region the spin conductances remain sizable, too. Further, we find that at small biases and for incoming currents being unpolarized, there are spin currents with opposite signs in each lead.

Upon a current flowing, spin accumulates in the vicinity of each contact as a consequence of the spin currents; the magnetizations at left and right contacts are the same and reverse with voltage and helicity. The magnitude of the accumulated spin polarization is directly proportional to the spin conductance of the respective lead; therefore, we reveal a new route towards the measurement of $G_z^{(\mathfrak{L}/\mathfrak{R})}$.

We add a remark on spin-accumulation in mesoscopic systems: accumulated spins have a feedback on the transport currents in first order in the applied biases. In particular, spin accumulations can drive charge currents as well as charge currents can drive spin currents, reflecting an Onsager reciprocity. Seemingly, this reciprocity has not been widely appreciated

in previous theories of the CISS effect.

The minimal model therefore directly reveals important features of analytic structure of spin transport in helical molecules. It can serve as a guidance for the interpretation of ab-initio calculations of transport coefficients in chiral molecular systems, *e.g.*, based on nonequilibrium Green's functions. Further, it lends itself to straightforward generalizations, e.g., the analytic calculation of current-induced mechanical torques in a quantum model.

Methods

The band-structure of an infinite helical wire was obtained by diagonalizing the Eq. (10). Explicit analytic expressions are given in the Supporting Information, Sec. S2. The junction was modelled with a central helical element of length L attached to a pair of semi-infinite straight tubes. Hamiltonian eigenstates were obtained by wavefunction matching, see Sec. S3. Spin conductances were obtained from the scattering matrix in Landauer approach; the respective formulæ were re-derived in Sec. S5 for reference purposes. The local magnetization density was calculated from explicit wave-functions in presence of two chemical potentials, Sec. S6.

Acknowledgement

Supporting Information Available: The accompanying file contains supporting sections S1-S6 with methodological details.

References

1. Evers, F.; Korytár, R.; Tewari, S.; van Ruitenbeek, J. M. Advances and Challenges in Single-Molecule Electron Transport. Rev. Mod. Phys. **2020**, 92, 035001.

2. Göhler, B.; Hamelbeck, V.; Markus, T. Z.; Kettner, M.; Hanne, G. F.; Vager, Z.; Naaman, R.; Zacharias, H. Spin Selectivity in Electron Transmission Through Self-Assembled Monolayers of Double-Stranded DNA. Science **2011**, 331, 894.

3. Naaman, R.; Paltiel, Y.; Waldeck, D. Chiral Molecules and the Electron Spin. Nature Reviews Chem. **2019**, 3, 250–260.

4. Liu, T.; Wang, X.; Wang, H.; Shi, G.; Gao, F.; Feng, H.; Deng, H.; Hu, L.; Lochner, E.; Schlottmann, P., et al. Linear and Nonlinear Two-Terminal Spin-Valve Effect from Chirality-Induced Spin Selectivity. ACS Nano **2020**, 14, 15983–15991.

5. Safari, M. R.; Matthes, F.; Caciuc, V.; Atodiresei, N.; Schneider, C. M.; Ernst, K.-H.; Bürgler, D. E. Enantioselective Adsorption on Magnetic Surfaces. Advanced Materials **2023**, 2308666.

6. Safari, M. R.; Matthes, F.; Schneider, C. M.; Ernst, K.-H.; Bürgler, D. E. Spin-Selective Electron Transport Through Single Chiral Molecules. Small **2023**, 2308233.

7. Theiler, P. M.; Ritz, C.; Hofmann, R.; Stemmer, A. Detection of a Chirality-Induced Spin Selective Quantum Capacitance in α-Helical Peptides. Nano Lett. **2023**, 23, 8280–8287.

8. Evers, F.; Aharony, A.; Bar-Gill, N.; Entin-Wohlman, O.; Hedegård, P.; Hod, O.; Jelinek, P.; Kamieniarz, G.; Lemeshko, M.; Michaeli, K., et al. Theory of Chirality Induced Spin Selectivity: Progress and Challenges. Adv. Mat. **2022**, 34, 2106629.

9. Wolf, Y.; Liu, Y.; Xiao, J.; Park, N.; Yan, B. Unusual Spin Polarization in the Chirality-Induced Spin Selectivity. ACS Nano **2022**, 16, 18601–18607.

10. Michaeli, K.; Naaman, R. Origin of Spin-Dependent Tunneling Through Chiral Molecules. J. Phys. Chem. C **2019**, 123, 17043–17048.

11. García-Blázquez, M.; Dednam, W.; Palacios, J. Nonequilibrium Magneto-Conductance as a Manifestation of Spin Filtering in Chiral Nanojunctions. J. Phys. Chem. Lett. **2023**, 14, 7931–7939.

12. Korytár, R.; Evers, F. Current-Induced Mechanical Torque in Chiral Molecular Rotors. Beilstein Journal of Nanotechnology **2023**, 14, 711–721.

13. Abragam, A. The Principles of Nuclear Magnetism; Oxford university press, 1961; Chapter II.B.

14. Geyer, M.; Gutierrez, R.; Cuniberti, G. Effective Hamiltonian Model for Helically Constrained Quantum Systems within Adiabatic Perturbation Theory: Application to the Chirality-Induced Spin Selectivity (CISS) Effect. J. Chem. Phys. **2020**, 152, 214105.

15. König, M.; Buhmann, H.; W. Molenkamp, L.; Hughes, T.; Liu, C.-X.; Qi, X.-L.; Zhang, S.-C. The Quantum Spin Hall Effect: Theory and Experiment. J. Phys. Soc. Japan **2008**, 77, 031007.

16. Sánchez, D.; Serra, L. m. c.; Choi, M.-S. Strongly Modulated Transmission of a Spin-Split Quantum Wire with Local Rashba Interaction. Phys. Rev. B **2008**, 77, 035315.

17. Středa, P.; Šeba, P. Antisymmetric Spin Filtering in One-Dimensional Electron Systems with Uniform Spin-Orbit Coupling. Phys. Rev. Lett. **2003**, 90, 256601.

18. Marganska, M.; Milz, L.; Izumida, W.; Strunk, C.; Grifoni, M. Majorana Quasiparticles in Semiconducting Carbon Nanotubes. Phys. Rev. B **2018**, 97, 075141.

19. Jacquod, P.; Whitney, R. S.; Meair, J.; Büttiker, M. Onsager Relations in Coupled Electric, Thermoelectric, and Spin Transport: The Tenfold Way. Phys. Rev. B **2012**, 86, 155118.

20. Bercioux, D.; Lucignano, P. Quantum Transport in Rashba Spin-Orbit Materials: A Review. Rep. Progr. Phys. **2015**, 78, 106001.

21. Ref. 20, Sec. 4.1.

22. Edelstein, V. Spin Polarization of Conduction Electrons Induced by Electric Current in Two-Dimensional Asymmetric Electron Systems. Solid State Communications **1990**, 73, 233–235.

23. Nazarov, Y. V.; Blanter, Y. M. Quantum Transport: Introduction to Nanoscience; Cambridge University Press, 2009.

24. Bardarson, J. H.; Adagideli, i. d. I.; Jacquod, P. Mesoscopic Spin Hall Effect. Phys. Rev. Lett. **2007**, 98, 196601.

25. Adagideli, i. d. I.; Bardarson, J. H.; Jacquod, P. Electrical Probing of the Spin Conductance of Mesoscopic Cavities. Journal of Physics: Condensed Matter **2009**, 21, 155503.

26. Adagideli, i. d. I.; Scheid, M.; Wimmer, M.; Bauer, G. E. W.; Richter, K. Extracting Current-Induced Spins: Spin Boundary Conditions at Narrow Hall Contacts. New Journal of Physics **2007**, 9, 382.

27. Liu, Y.; Xiao, J.; Koo, J.; Yan, B. Chirality-Driven Topological Electronic Structure of DNA-Like Materials. Nature Mater. **2021**, 20, 638–644.

28. Adachi, Y.; Ohshita, J. Germanium and Tin in Conjugated Organic Materials. Main Group Strategies towards Functional Hybrid Materials **2017**, 237–264.
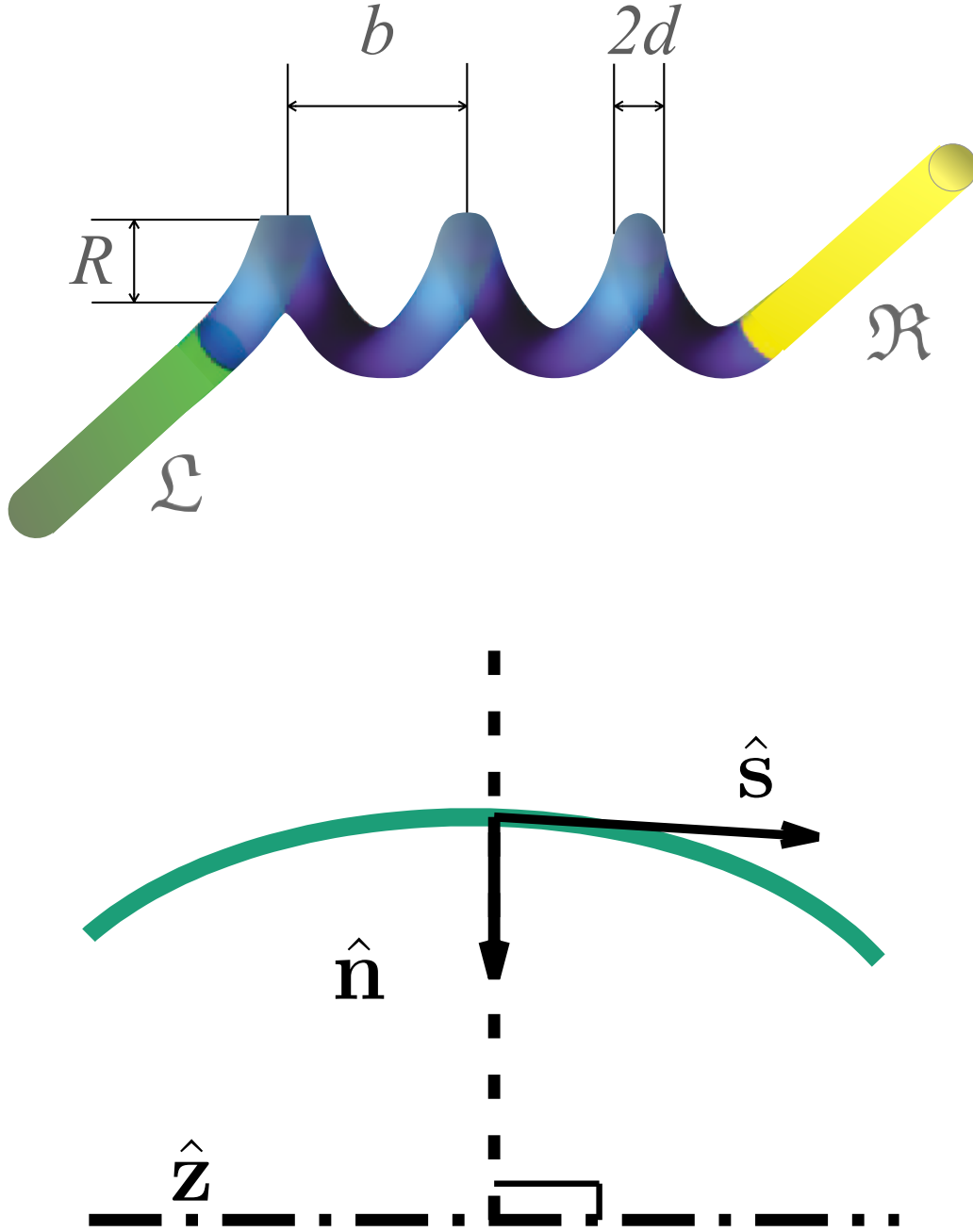
TOC Graphic
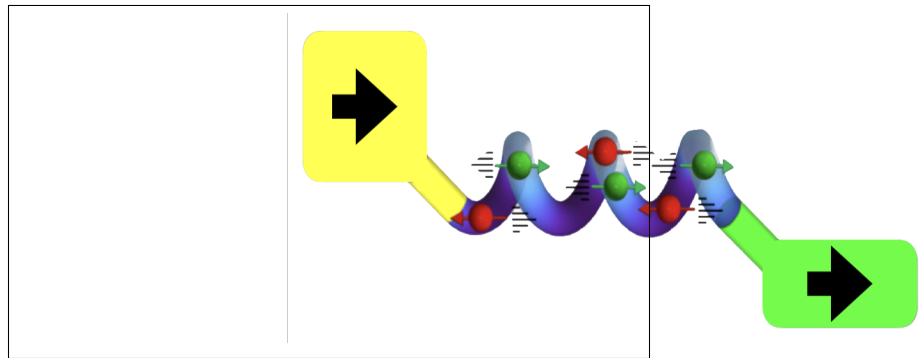
Figure 1: Top: Scheme of the molecular junction consisting of a helical tube (center) and a pair of semi-infinite straight tubes, left and right. The radius R, pitch b, thickness $2d$ are indicated. Bottom: Illustration of helical coordinates s, ϱ, θ: Green line shows part of a helix that evolves along the z axis (dash-dotted line) with unit vector $\hat{\mathbf{z}}$. At any given point on the helix, the unit vector $\hat{\mathbf{n}}$ is perpendicular to $\hat{\mathbf{z}}$ and the unit tangent vector $\hat{\mathbf{s}}$. In helical coordinates, s is the distance along the helix; θ and ϱ are polar coordinates in a plane normal to $\hat{\mathbf{s}}$; θ measures from $\hat{\mathbf{n}}$.
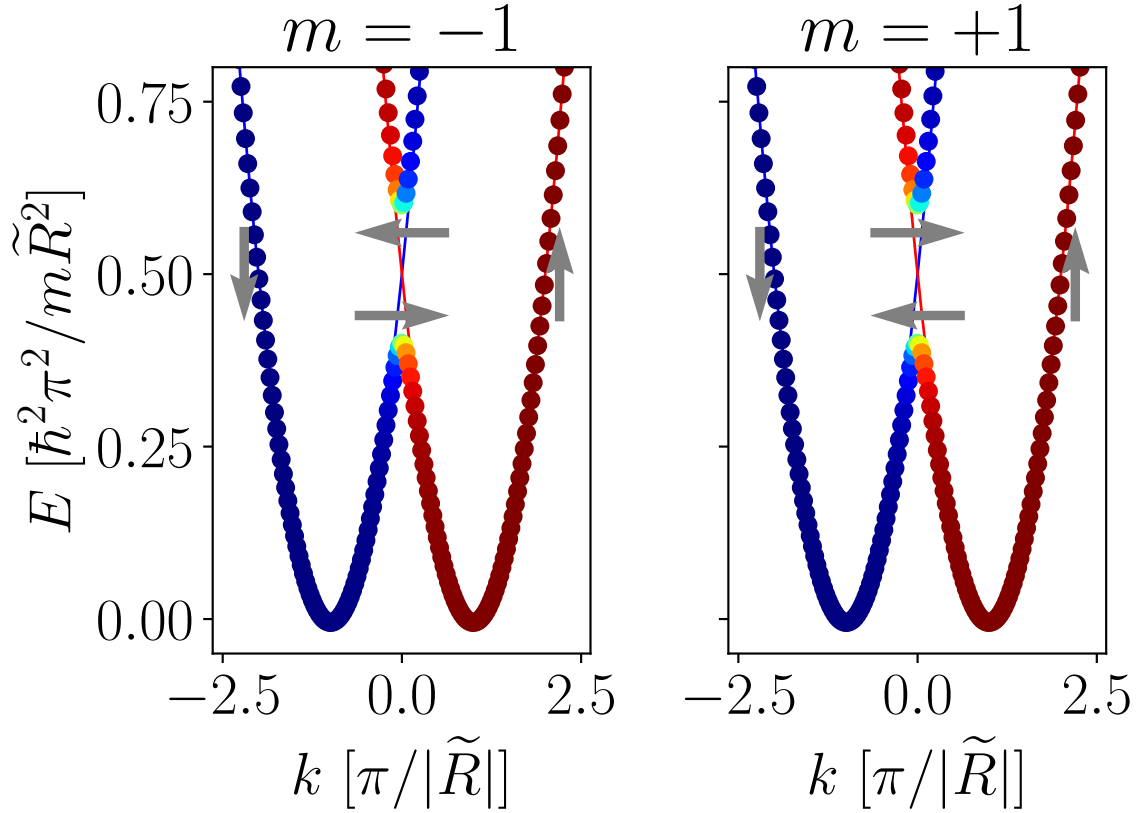
Figure 2: Dispersion relation of the helical tube for $m = +1$ and -1 is shown with dots. Color indicates the expectation value of $\hat{\sigma}_z$ (red=+1, blue=-1, green=0). Grey arrows represent the expectation value of spin in the yz-plane [$\hat{\sigma}_y$ ($\hat{\sigma}_z$) is the horizontal (vertical) component, respectively]. For comparison, the thin solid lines depict the dispersion of a straight tube. The horizontal spin-dependent shift of the parabolæ reflects the non-Abelian gauge transformation. Parameters: $\tilde{\kappa} = 0.1, \lambda = -1$. The eigen-energies are m-independent.
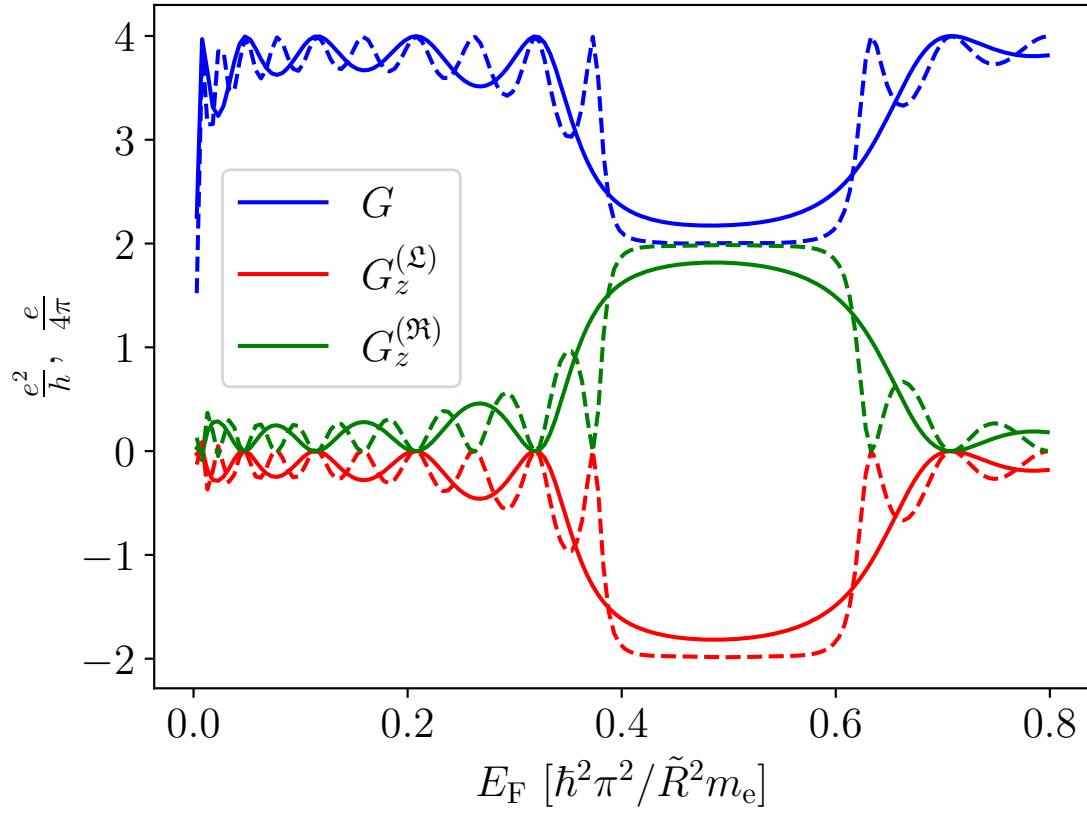
Figure 3: Charge conductance and the z-components of the spin conductances in the Michaeli model as a function of the Fermi energy E_F. Solid (dashed) lines are for a helix with 3 (dashed) and 6 (solid) turns. Parameters are the same as in Fig. 2, with a spin-orbit gap between 0.4 and 0.6.
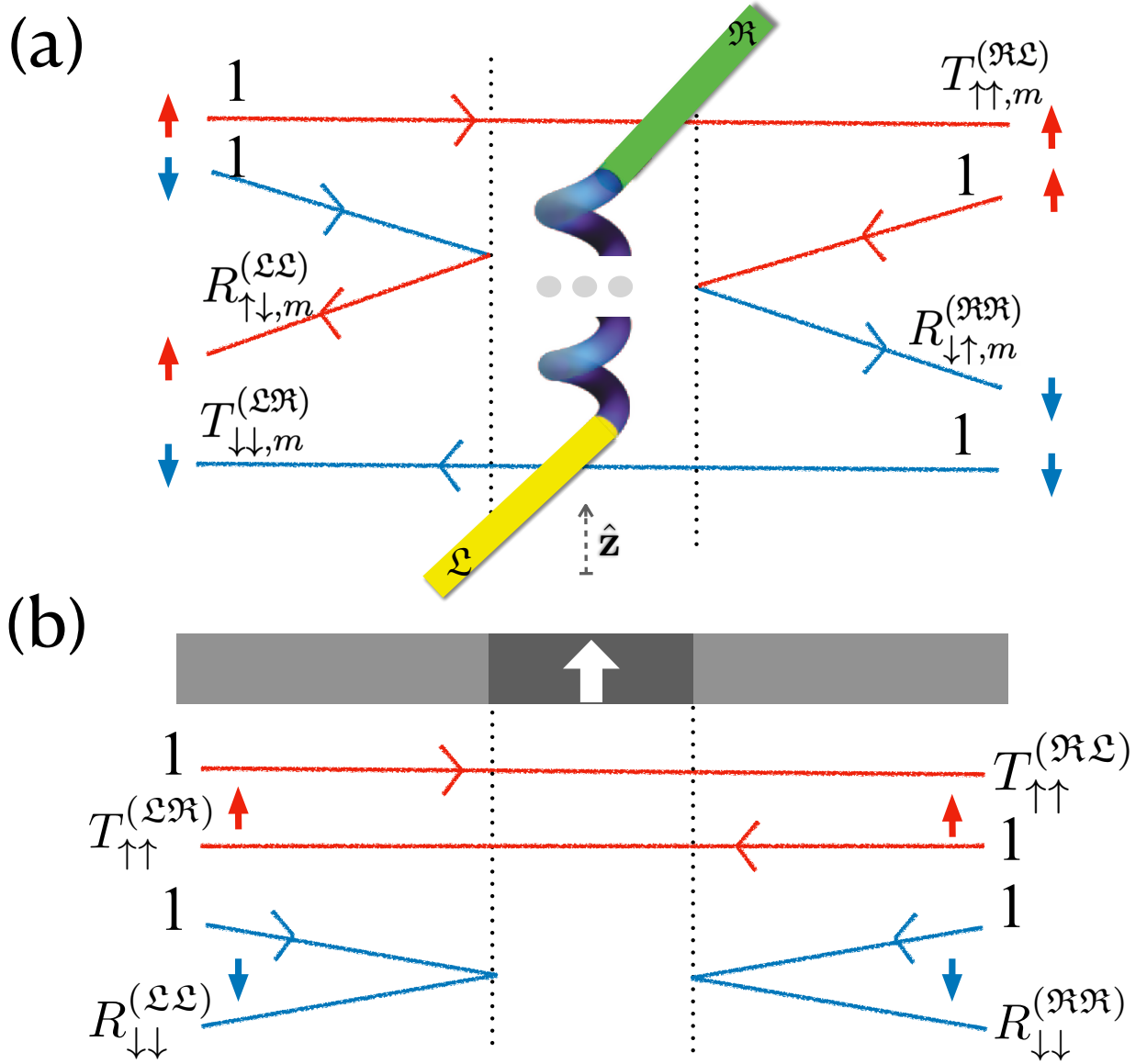
Figure 4: Schematic representation of scattering processes in the helical junction (a) and a ferromagnetic polarizer (b). Panel (a) applies in the limit of a long helix (helicity $\lambda = -1$) for energies in the spin-orbit gap. Red (blue) color indicates spin up (down) in the sense of the helical axis. The red line on the top indicates that the electron with spin $\uparrow$ coming from the left ($\mathfrak{L}$) lead (normalized to probability 1) is transmitted and its spin is conserved. If the incoming electron has spin $\downarrow$, it is reflected with a spin-flip due to TRI. Panel (b) illustrates scattering off an ideal ferromagnetic polarizer that only transmits spin up electrons.
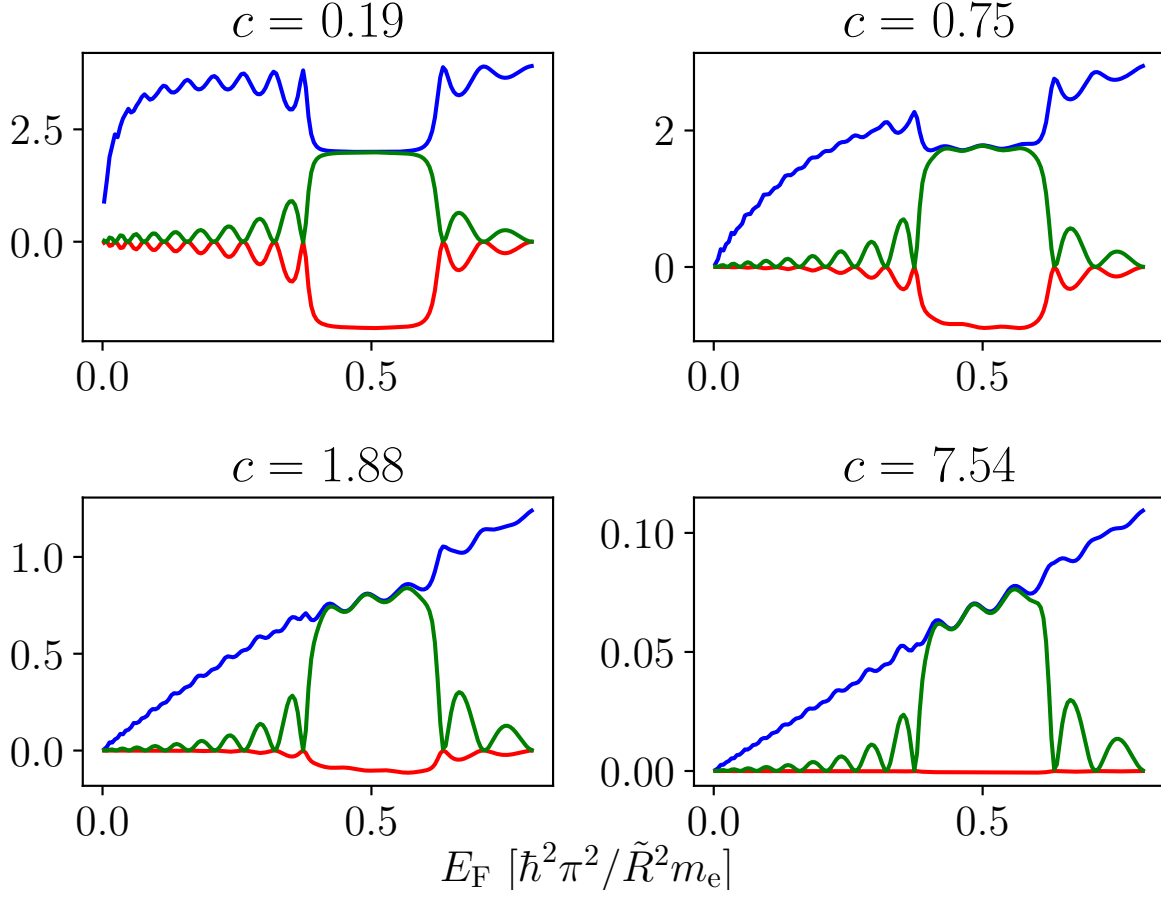
Figure 5: Plot similar to Fig. 3 illustrating the sensitivity of charge and spin conductances, $G/\frac{e^2}{h}$ (blue), $G_z^{(\mathfrak{R}/\mathfrak{L})}/\frac{e}{4\pi}$ (green/red) to the contact imperfection (14) for a helical wire with 6 turns. The panels differ by increasing strength of the potential barrier c at the left contact.